Dimensions and entropies of chaotic intensity pulsations in a single-mode far-infrared NH_3 laser

U. Hübner, N. B. Abraham,* and C. O. Weiss
Physikalisch-Technische Bundesanstalt, Bundesallee 100, D-3300 Braunschweig, Federal Republic of Germany
(Received 17 April 1989)

Detailed studies of digitized recordings of periodic and chaotic intensity pulsing of an unidirectional far-infrared NH_3 ring laser at 81.5 μm reveal common features of a broad range of different pulsing patterns as well as systematic relationships among entropies, dimensions, and decay rates of the autocorrelation function. Spiral-type "Lorenz-like" chaos of many different spiraling rates and of differing modulation depths has an underlying attractor dimension of 2.0–2.3 and an entropy rate that lies mainly in the range $(0.2–0.7)T^{-1}$, where T is the average intensity pulsing period. Over a wide range of types of pulsing (spiral chaos, period-doubling chaos, and periodic states) the decay rate of the envelope of the autocorrelation function over short times provides an estimator of the entropy. The results are in excellent agreement with the characteristics of the Lorenz-Haken model for similar operating parameters.

I. INTRODUCTION

Periodic and chaotic self-pulsing has been observed in NH_3 FIR (far-infrared) single-mode lasers.[1] Many of the characteristics (thresholds, period-doubling sequences) of this pulsing for relatively high-pressure operation have been in agreement with predictions from the Lorenz-Haken model for a single-mode laser with a homogeneously broadened two-level medium.[2–4] At lower pressures three-level coherence effects seem to become relevant, indicating their presence by lower pulsing thresholds, supercritical Hopf bifurcations, and homoclinic chaos.[5]

The formal justification of modeling optically pumped FIR lasers (in the high-pressure regime) by the simple Lorenz-Haken model has been widely disputed[6–11] because the coherent optical pumping appears to prevent reduction of models for the three-level FIR laser to the simpler form for a two-level system. However, none of the more complex models proposed is yet as complex as the FIR laser. In particular, large angular momentum states of the relevant molecular levels are involved and the angular momentum m sublevels are mixed by the orthogonal linear polarizations of the pump and FIR fields. In addition, transverse and longitudinal profiles of the pump and FIR beams have not yet been incorporated in the theories. The most complex of the alternative models considered (that of Ref. 11 which involves as may as 1000 equations) closely approaches the experimental results in terms of instability thresholds and intensity pulsing patterns, but differs in some more subtle characteristics which have been resolved only recently by phase-sensitive measurements of the laser amplitude.[5]

Chaotic pulsing corresponds to motion on strange attractors which can be identified and characterized by dimensions, entropies, and Lyapunov exponents.[12–18] In order to quantitatively characterize the chaotic pulsing of the FIR laser, we have applied the methods of Grassberger and Procaccia to calculate the dimension (D_2) and the associated entropy (K_2) which are lower bounds and generally good estimators of the fractal dimension (Hausdorff dimension) of the strange attractor and of the Kolmogorov entropy of the signal. The signal-to-noise ratio with which the chaotic pulses are recorded in this experiment exceeds 250 in the observation bandwidth. It is thus adequate for full use of the eight-bit resolution of the fast transient digitizers with large storage capacity which are presently available. Signals of this quality have so far not been available for statistical analysis of chaos in autonomous laser systems. We can therefore calculate dimensions and entropies of the laser pulsing for comparisons with the results from various theoretical models.

The paper is organized as follows. In Sec. II we describe the laser, the measurement system, and the recorded intensity pulsing patterns. In Sec. III we illustrate the analysis procedures for sample data sets. Dimensions, entropies, autocorrelation times, pulsing periods, spiraling rates, and other characteristics of the many different data sets are compiled and discussed. The results are compared with those from the analysis of similar data records generated by the numerical solution of the Lorenz equations in Sec. IV. Discussion of the results is provided in Sec. V.

II. EXPERIMENTAL SETUP AND DATA SAMPLES

The measurements were made on an 81.5-μm $^{14}NH_3$ cw (FIR) laser, pumped optically by the $P(13)$ line of an N_2O laser via the vibrational $aQ(8,7)$ NH_3 transition. The basic laser setup is shown in Fig. 1 and is essentially identical to that used in Ref. 1. As in Ref. 1 stable pump conditions were achieved by control of the pump laser frequency with respect to the Lamb dip of the $aQ(8,7)$ NH_3 absorption line center using an NH_3 Lamb dip cell. Detuning of the pump laser frequency leads to different

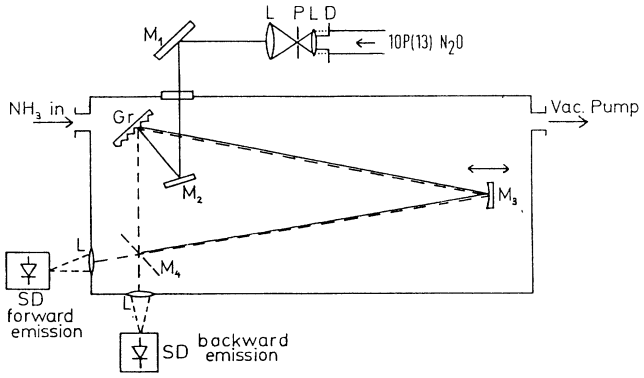

FIG. 1. Ring laser for observation of chaotic laser dynamics. *M*: mirrors; Gr: 10-μm grating; SD: Schottky-barrier diodes used as detectors. The usual coupling holes which perturb modes are avoided by in coupling of the pump radiation via a grating and out coupling via a mesh reflector. Pumping is by a 10.7-μm N_2O laser. The wavelength generated is 81.5 μm. The pump beam is attenuated without change in geometry, direction, or frequency by a combination of a spatial filter [lens, pinhole diaphragm, lens (*LPL*)] and iris (diaphragm *D*).

resonant frequencies for forward and backward traveling waves (forward denotes FIR emission copropagating with the pump light) which are fully separated when the detuning exceeds the homogeneous linewidth. Laser emission in the direction opposite to the pump beam propagation can thus be achieved by tuning resonator length into resonance with the backward wave only. The backward emission line shows no ac Stark splitting (though there is ac Stark broadening). The emission in the direction of the pump beam propagation nevertheless was monitored to assure that there was no bidirectional emission while the data were taken. The backward emission of the FIR laser was detected by a micrometer-sized Schottky-barrier diode. The resulting intensity pulsing when observed on a spectrum analyzer had a spectral signal-to-noise ratio as much as 70 dB in 100-kHz bandwidth. This corresponded to a signal-to-noise ratio of about 300:1 in terms of peak pulse height to rms noise. For numerical analysis the signals were digitized with 8-bit resolution, an interval of 40 ns between samples, and 25 000 samples per recording.

The experimental parameters are the pump intensity, FIR laser pressure, and FIR laser cavity tuning but for comparison with the Lorenz-Haken model it is important to also know the decay rates. The most "Lorenz-like" pulsing could be found at the highest pressure (about 10 Pa) which still gave pulsing. At this pressure the gain linewidth is about 1 MHz wide, and the pulsing frequencies observed were of this order. This leads us to infer that the cavity linewidth was probably not more than two or three times larger. It is known for the NH_3 transition used that the ratio of the population and polarization decay rates is 0.25.[19] At higher pressures than 9 Pa no pulsing was observed in the normal resonator setup. However, pulsing could be restored at these higher pressures by increasing the resonator losses (using an iris in the resonator) which gives clear evidence that the pulsing arises after passing through a "bad cavity" instability.

Laser pulsing was recorded for different pump intensities, NH_3 pressures, and FIR cavity detunings (see figure captions for values). The first two of those parameters could be reliably determined but the detuning values are less precise since they are taken from mechanical resonator length readings, which are affected by mechanical hysteresis (resonator length changes are in the submicrometer range).

Short sections of different time series are shown in Figs. 2 and 3. Figure 2 shows a variety of measured "spiral" (intermittent) chaotic pulsing (in the following called "Lorenz-type chaos") found for near resonant tuning of the FIR laser cavity. They differ notably in the length and modulation depth of the envelope of successive spirals. Differences in the spirals result primarily from changes in the NH_3 pressure in the range of about 8 to 10 Pa. Unusual features are seen between the last large pulse and the very beginning of the next spiral, e.g., broad gaps, where oscillation is suppressed up to one pulse length (see trace *c*), small kinks before the start of the spirals (end of traces *d* and *e*), or overshooting com-

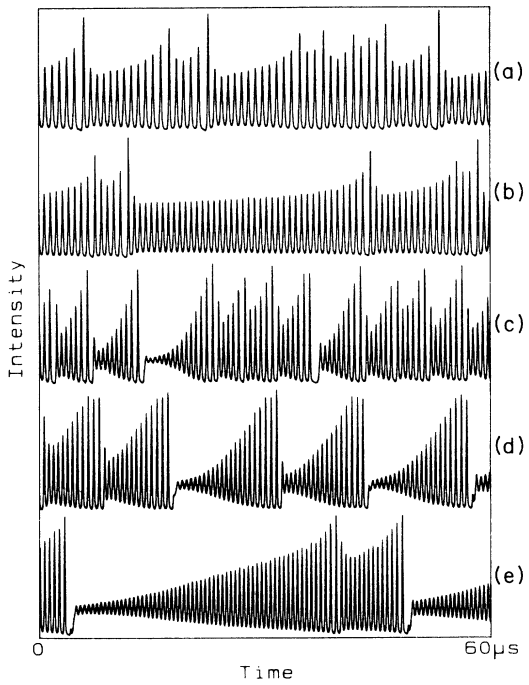

FIG. 2. Spiral-type pulsing of the laser intensity. The pressure varied for cases (a)–(e) from 8 to 10 Pa and the pump intensity was about 14 times above threshold. Resonator tuning was kept as constant at line center as experimentally possible. 1500 samples were plotted per trace. The average pulsing frequency increases from about 1.05 MHz (about 25 samples per pulse) for trace *a* to about 1.7 MHz (about 15 samples per pulse) for trace *e*. Successive traces are offset vertically for clarity.

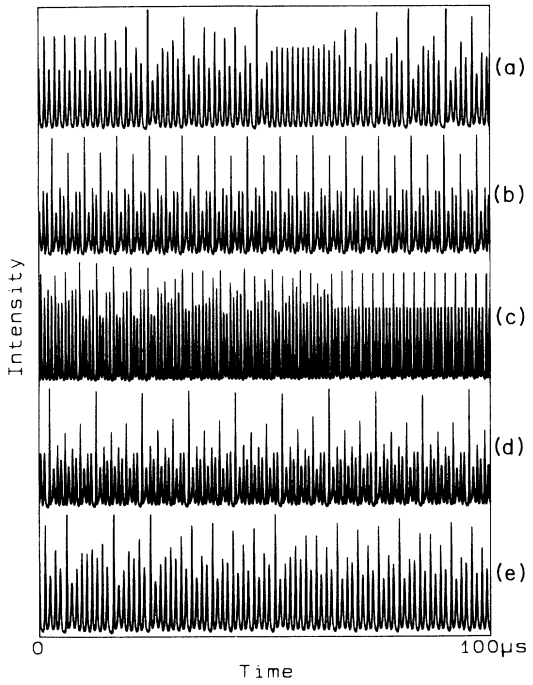

FIG. 3. Periodic and period-doubling chaotic pulse trains for the detuned laser resonator with different detunings around $\delta \approx 0.2$. The pressure was held constant at 9 Pa and the pump intensity was the same as in Fig. 2. 2500 samples are taken per trace. Case (a): Onset of period-doubling chaos; case (b): stable period 8; case (c): inverse period-doubling to the stable period-3 window; case (d): stable period 12; case (e) period-doubling chaos. Successive traces are offset vertically for clarity.

pared to the next smaller pulses (midway in trace *d*). The pulsing frequency increases from 1.05 MHz (about 25 samples per pulse) for trace *a* to 1.7 MHz (about 15 samples per pulse) for trace *e*, primarily because of differences in gas pressure.

Figure 3 shows periodic pulsing and a closely related form of chaotic pulsing (in the following called "period-doubling chaos") which were observed by detuning of the laser resonator. These include the onset of period-doubling chaos (traces *a* and *e*), stable period 8 (trace *b*), period 5 (see first third of trace *c*) which by inverse period doubling (perhaps because of a drifting parameter) switches to period 3, and stable period 12 (trace *d*). Simple periodic traces such as period 2 or 4 have been recorded but are not shown.

III. ANALYSIS OF DATA

Several methods[12,13,20] were used to analyze the physical properties of the different data sets. Figure 4 presents three typical data sets called Lorenz-type chaos (data set 5), period-doubling chaos (data set 10), and period-2 pulsing (data set 7).

Portions of the intensity time series shown in row 1 can be used to discriminate roughly between periodic, period-doubling chaotic, and Lorenz-type chaotic pulse trains. For more precise identification and characterization we have used "phase portraits" (row 2), autocorrelation functions (row 3), log-log plots of the correlation integral C of Grassberger and Procaccia[12] (row 4), and its slope (row 5). The latter two have been used to determine the correlation dimension D_2 and the second-order entropy K_2.

The term phase portrait is used for a two-dimensional plot of the 8-bit data x_i ($i=1,2,\ldots,25\,000$) in the form of x_{i+k} versus x_i. For different values of the delay k one obtains some insight into the spatial structure of the attractor underlying the data set, as different delays provide different views of the attractor, by a process equivalent to looking at the attractor in phase space under different viewing angles. One can understand a spatial cluster of points by looking at other angles which may reveal that a thickened line is the side view of a flat structure [see Fig. 5(f)] or of nearly periodic and nearly coplanar structures [see Figs. 5(a) and 5(b)]. One can also judge how point density variations are responsible for anomalous (nonfractal) structures see in the slope of the correlation integral C.

Figure 5 shows examples of phase portraits for three types of pulsing recordings. Parts (a) and (b) contain in each case the same 25 000 data points of a period-8 signal for delays 3 [case (a)] and 20 [case (b)]. The period-8 structure of the data is far better resolved in case (b). Parts (c) and (d) also contain in each case the full data set of 25 000 points for period-doubling chaos, again with the delay $k=3$ for case (c) and delay $k=28$ for case (d). The underlying attractors of period-doubling chaos have a "hole" determined by the smallest pulses [cases (a) and (c)] if the delay is of order $\frac{1}{4}$th of a period, but for other delays the attractor appears folded in a very strange manner [case (d)] with flat parts like wings of different orientation in phase space. A hole also occurs for Lorenz-like spiral chaos when the trajectory does not encroach on the vicinity of the unstable fixed point of constant intensity, i.e., each spiral begins with significant modulation. The last two figure parts [(e) and (f)] belong to a data set of Lorenz-type chaos. 25 000 data points are plotted for delay 2 [case (e)] and 15 [case (f)]. Here the signal looks like case (c) of Fig. 2 where the laser field comes close to the fixed point and thus practically no hole is observed [case (e)]. The structure of the pertinent attractor seems to consist of two leaves, one nearly perpendicular to the other [case (f)].

The autocorrelation function (ACF) of the data also provides insight into the structure of the attractors. It is normalized to unity for zero delay τ using the definition

$$R(\tau)=\frac{[\langle I(t)I(t+\tau)\rangle-\langle I(t)\rangle^2]}{[\langle I(t)^2\rangle-\langle I(t)\rangle^2]}\ .$$

The maximum delay plotted is $\tau=2000\Delta t$, where Δt is the time spacing between two adjacent samples.

We define a correlation time τ_c by fitting the first few peaks (and thus the envelope) of the autocorrelation function $R(\tau)=\exp(-\tau/\tau_c)$. For our 17 chaotic data we find

τ_c is in the range of about $2T$ to $6T$ (see Table I), where T is the period defined by the location of the first peak in the ACF. The rather high value for data set 26 results from the nearly perfect periodic pulsing parts contained in it. The envelope of the autocorrelation function decreases rather rapidly but there are significant differences in the overall structure of the ACF's of Lorenz-type and period-doubling chaos. All 15 Lorenz-type autocorrelation functions show the typical small groups of peaks growing ("revivals") and decreasing nonperiodically as found by numerical investigations of the Lorenz equations.[21] Clearly length, amplitude, and separation of the

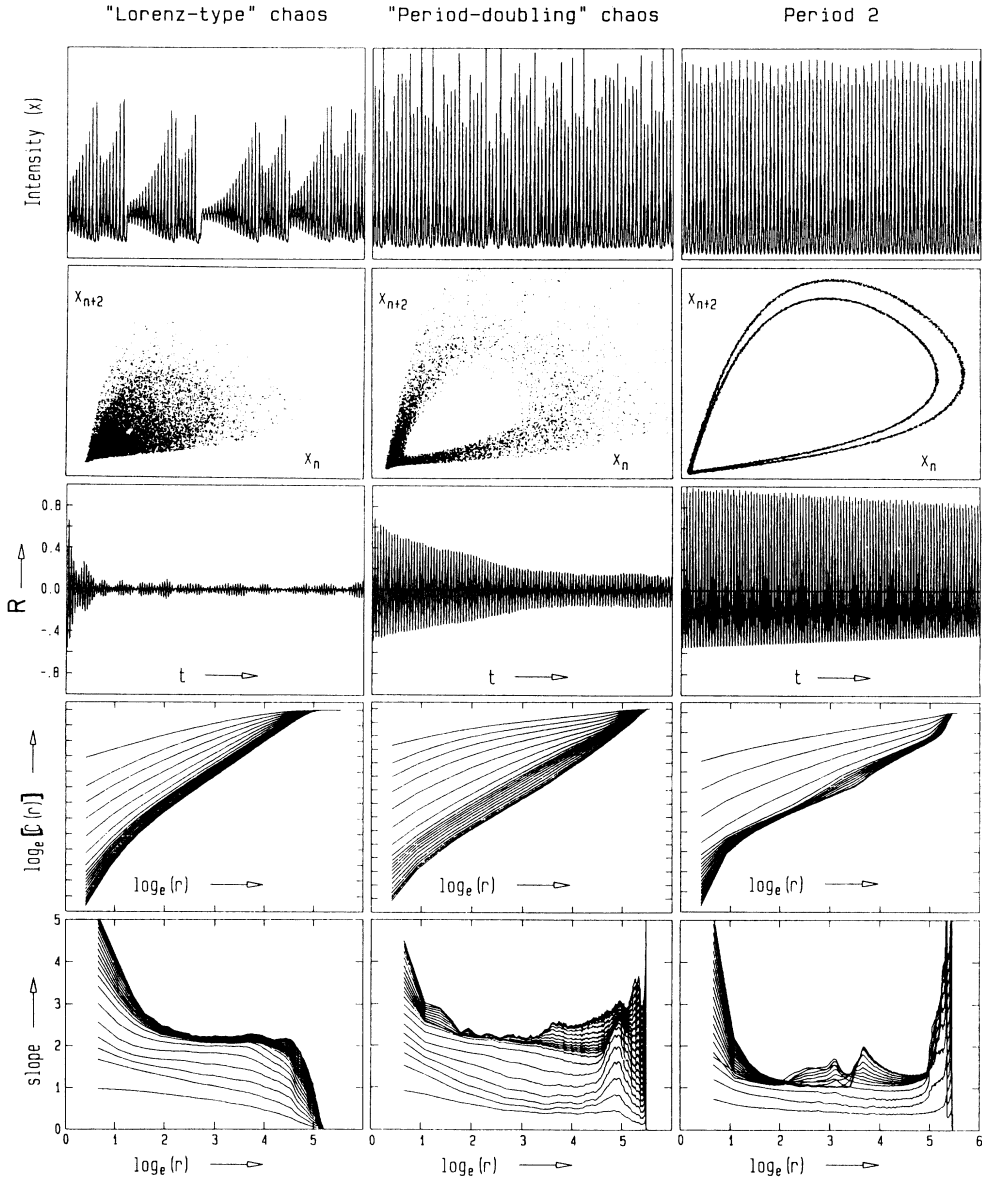

FIG. 4. Comparison of data sets for the various methods used to analyze the experimental data. Columns 1, 2, and 3 are for data sets 5 (pressure ≈ 8 Pa, same pump intensity as in Fig. 2, detuning $\delta \approx 0$), 10 (pressure 9 Pa, same pump intensity as in Fig. 2, detuning $\delta \approx 0.2$), and 7 (pressure 9 Pa, same pump intensity as in Fig. 2, detuning $\delta \approx 0.2$) as collected in Table I. Row 1: pulse trains of characteristic data sets with 1500 samples per column. Row 2: phase portraits (25 000 data; delay $k = 2$; $T/\Delta t$ values in Table I); row 3: autocorrelation functions (maximum delay: 2000 sample spacings; maximum vertical scale: 1.0). Row 4: log-log (base e) plot of the correlation integral vs length scale r for embedding dimensions 1 to 20 (upper to lower); row 5: slopes of the log-log plots of the correlation integral vs $\log(r)$ for embedding dimensions 1 to 20 (lower to upper).

groups of oscillations differ slightly among those 15 data sets but the overall structure compares favorably with the calculation.

On the other hand no such groups of oscillations are found with the ACF's of the period-doubling chaos data sets. This completely different overall behavior can be seen in column 2 of Fig. 4 Despite a relatively small correlation time τ_c (see Table I, data set 26) a much longer second characteristic time of moderate correlation is also found. Because we recorded only a small number (2) of data sets identified as period-doubling chaos, a confirmation that this behavior is characteristic of such ACF's is not safely established.

Rows 4 and 5 of Fig. 4 show examples of the correlation integral C and its slpoe versus the distance r. C is calculated, as mentioned previously, using the method of Grassberger and Procaccia.[12] This method analyzes a single-variable time series by constructing representations of the attractor in E-dimensional phase spaces using the time-delay method as discussed, e.g., by Froehling *et al.*[22] They define

$$\mathbf{X}(t)=(x(t),x(t+\tau),\ldots,x(t+(E-1)\tau)) ,$$

where $\mathbf{X}(t)$ is a vector built up out of E consecutive samples of the time series with successive time delays $\tau=n\cdot\Delta t$, n being an integer. For discrete samples x_i the correlation integral C becomes

$$C(r)=\lim_{N\to\infty}\left[\frac{1}{N(N-1)}[\mathcal{N}(i,k),\|\mathbf{X}_i-\mathbf{X}_k\|<r]\right] . \quad (1)$$

$\mathbf{X}_i$ (similarly $\mathbf{X}_k$, $k\neq i$) mean vectors $(x_i,x_{i+n},x_{i+2n},\ldots,x_{i+(E-1)n})$, $\mathcal{N}(i,k)$ is the number of pairs (i,k), and $\|\mathbf{X}_i-\mathbf{X}_k\|$ is of the norm of the vector difference. E is called the "embedding dimension." The choice of the norm is of practical importance for data sets such as ours, although in Eq. (1) the Euclidean norm (length of the difference vector) and the maximum norm give the same correlation dimension D_2 and entropy K_2.[23] To reduce the time necessary to compute the correlation integral C for 25 000 data and 20 embedding dimensions ($1\le E\le 20$) we chose the maximum norm

$$\|\mathbf{X}_i-\mathbf{X}_k\|=\max_{0\le m\le E-1}|x_{i+m}-x_{k+m}| . \quad (2)$$

In practice, one infers the existence of an attractor when one observes a plateau region in the slopes of the correlation integral, where the flatness of the plateau is interpreted as evidence for a self-similar scaling region of fractal dimension and where the convergence of the slopes with increasing embedding dimension indicates the

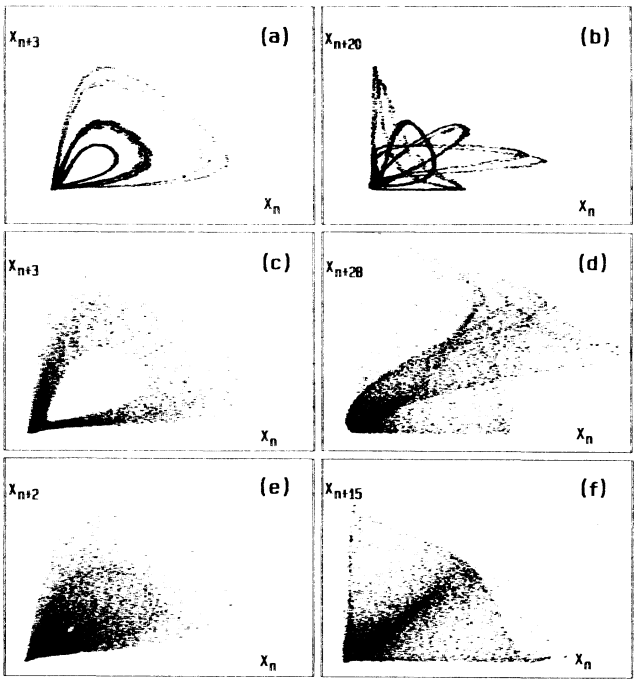

FIG. 5. Characteristic phase portraits for period-8 [cases (a) and (b) with delays $k=3$ and 20 for data set 23, pressure 9 Pa, pump intensity as in Fig. 2, detuning $\delta\approx 0.2$], period-doubling chaotic [cases (c) and (d) with delays $k=3$ and 28 for data set 10, pressure 9 Pa, pump intensity as in Fig. 2, detuning $\delta\approx 0.2$], and Lorenz-type chaotic [cases (e) and (f) with delays $k=2$ and 15 for data set 5, pressure 9 Pa, pump intensity as in Fig. 2, detuning $\delta\approx 0$] pulsing. 25 000 data were used.

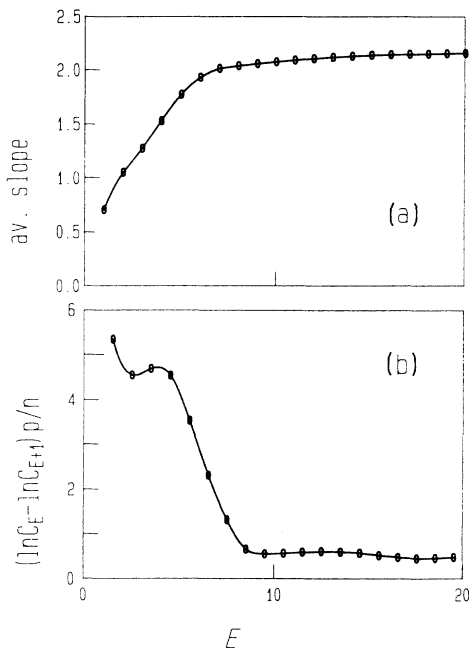

FIG. 6. (a) Average slope in the "plateau region" versus embedding dimension E for data set 5 (see column 1 of Fig. 4 for parameter values). The correlation dimension D_2 is taken as the value for embedding dimension 15. (b) $[\ln(C_E)-\ln(C_{E+1})]p/n$ vs embedding dimension E; p is the average number of data samples covering the average pulsing period and n (integer) means the delay between successive components of each vector $\mathbf{X}_i$. The entropy K_2 per average pulsing period T, K_2T, is taken as the estimated asymptotic from the highest values of E.

reconstruction of a topologically unique attractor. One sees such a plateau in Fig. 4, row 5, and as an example for the Lorenz-type chaos, the average in the scaling region is plotted in Fig. 6(a). One also sees that for $E \gtrsim 6$ the value converges to slightly more than 2.0. A slow increase in this plot with E for large E reflects an unavoidable effect of the presence of noise. An analysis of these effects is given elsewhere.[24]

While, in principle, the method does not depend on the choice of τ, practical considerations of precision, noise, and exponential divergence limit satisfactory values of τ. As an estimate of the best value of the time delay τ, respectively, n, we have found for our data sets that if τ is not too large there is a relation $\tau E_c \approx T$ between τ, the average pulse period T, and the embedding dimension E_c which marks the onset of the convergence of the slope curves and which, on the other hand, signals convergence of the method. It reflects the fact that the structural information used to reconstruct attractors which are nearly two dimensional is connected with the time interval $(E-1)\tau$ of the data set covered by the vector and not with the individual choices of E or τ.[25,26] Moreover, after one revolution of the attractor the succeeding orbits come close to the previous one so that the benefit for structural information is small if E or τ are increased further.

Considering various arguments and after some empirical trials, we settled on $\tau \approx T/7$ as a best value (which led to $n=2$ or $n=3$ for our data sets).

Equations (1), (2), and the relation[12,25]

$$C(r) \sim r^{D_2} e^{-E\tau K_2}, \tag{3}$$

which holds for $r \to 0$ and $E \to \infty$, were then used to calculate D_2 and K_2. The 8-bit data can have integer values between 0 and 255 and thus so also do the absolute values of the component differences. Thus r lies in the interval $0 \le r \le 255$ which results in an interval of $0 \le \ln(r) < 6$ on the natural logarithmic scale. The plateau area of the converging slope curves was averaged and corresponds to a D_2 of slightly above 2 for the Lorenz-type and the period-doubling chaos or to $D_2 \approx 1$ in case of the period-2 signal. K_2 was calculated by dividing $C_E(r)$ and $C_{E+1}(r)$ [see Eq. (3)] which results in $\ln(C_E) - \ln(C_{E+1}) = \tau K_2$. Numerically $\ln(C_E)$ and $\ln(C_{E+1})$ were calculated from the average straight line in the plateau area for a value of r in the center of this interval

The plots in rows 4 and 5 of Fig. 4 contain a special correction which we call the "shift correction." This means that the correlation integral $C(r)$ is plotted versus $r+p$ where p is half the least significant bit. This is the most straightforward way to correct for the errors in the calculation of C resulting from the rounding of the data by the digitizer.[24] On average this correction procedure increases the slopes of $C(r)$ in the plateau region (correcting for the erroneous bias resulting from using 8-bit data) and thus increases the calculated estimate of D_2 by about 5% but it does not change K_2.

Some more remarks are necessary about characteristic features of the plots in row 5 of Fig. 4. All slope values were calculated from the difference of two adjacent values of $\ln(C_E)$ divided by the difference of the corresponding values of $\ln(r)$ and then centered onto the midpoint between those $\ln(r+p)$ values. This is the reason that the slope curves do not start at the vertical axis. The calculated values of the slope were then connected by straight lines as a guide to the eye to discriminate between results for different values of E.

For small r, as r decreases towards zero, the curves in row 5 of Fig. 4 (slopes) increase. An analysis shows[24] that this increase is caused by noise and is proportional to E/r^2 because, in each case, noise blurs the attractor into the available E dimensions, increasing to infinity for $E \to \infty$. The noise-induced increase in the curves also increases the slopes (plotted in row 5) in the plateau region, which is the explanation for the continued slight increase with E of a few percent in the average slope values as shown in Fig. 6. There the average slope in the plateau region is plotted versus E showing a clear onset of convergence at about $E \approx 7$. All data for D_2, presented in Table I, were then taken for embedding dimension $E=15$. This choice is somewhat artificial but is a compromise of looking for the best estimate of D_2 in spite of the noise influence, and treating all of our data sets consistently.

Besides the influence of noise there is another structure on the slope curves even in the plateau area. Especially at the largest r values, moderate or high peaks appear and grow with increasing E. That structure may be interpreted in two ways. First, density variations, easily seen in our phase portraits, cause variations in the differential increase of $C(r)$ with r. A second reason for this structure is connected with our choice of the maximum norm. It sharpens the frequency with which extreme values of the distance appear in contrast to the Euclidean norm which gives somewhat smoother variations of the density of interpoint distances.

Further structure sometimes shows up (see row 5 of Fig. 4, column of period-doubling chaos) for intermediate values of r. The steps and peaks on those slope curves may be residuals of the period-doubling scenario leading to this type of chaos. Periodic orbits lead to slope values of one but when period doubling happens the developing period-doubling Cantor set transverse to the periodic orbit leads to sudden increases in the density of points when new layers of the periodic orbits are crossed and thus slope values higher than one will be seen as steps and peaks becoming more and more. They are rounded by the smooth curvature of the continuous variable flow on the attractor and by noise that one finds a significantly higher dimension than one. Indeed, one finds the value characteristic of the accumulation point of a period-doubling sequence which is 1.55.[27,28]

The consequences of the mechanisms which produce the above-mentioned structure in the slope are that it is not smeared out by taking more and more data. Thus the determination of a region which can be interpreted as a plateau might be difficult or even impossible.

Figure 6(b) shows $(\ln C_E - \ln C_{E+1})p/n$ versus E. It provides an estimate of K_2 which is taken from the converging part for $E \gtrsim 10$. Circles mark the calculated values which are connected by a Lagrange interpolation

curve of third order to make the shape of the curve more pronounced, as was done in Fig. 6(a). The main point of Fig. 6(b) is that the values converge well above $E \approx 10$. But there is again a structure which may be interpreted as residual influence of the average period of the intensity pulses. Two maxima are found in this curve, one at $E \approx 4$ and the other at $E \approx 12.5$. The difference $\Delta E \approx 8.5$ when multiplied with the time difference used, $\tau = 2\Delta t$, between the vector components, gives a period of $17\Delta t$ which is very close to the average pulse period $17.5\Delta t$ of that data set. Because of those oscillations, the estimated values of K_2 contain some uncertainty. The high amount of computation time, necessary to calculate data up to, e.g., $E = 40$, prohibited more accurate evaluation of K_2. These oscillations and the slower convergence of K_2 with E than was observed for D_2 versus E are consistent with the observations of others. We also find that the condition for convergence of K_2 requires vector spans $(E-1)n\Delta t$ which are 5–10 times larger than E_c.[25,26]

All data, estimated by these procedures, are collected in Table I. Two data sets were not included, nos. 9 and 11. They consist of long parts alternating between periodic and chaotic behavior. We think that their average dimension, entropy, etc., would not yield any valu-

TABLE I. Collection of the most important results of the different experimental data sets with comparison to results of the numerical integrated Lorenz equations. The data sets are sorted such that the uppermost seven rows stand for data sets with periodic pulsing (P2,P4, . . .), the next two rows stand for period-doubling (PDC), and the other rows for Lorenz-type (LC) chaotic data sets. Theoretical values are added in the last four rows for comparison. p is the average number of samples per pulse period, τ_c is the decay constant of the autocorrelation function. C, WI, and I denote "constant," "weakly increasing," and "increasing" which reflects the behavior of the last 10 points of the average slope curve versus the embedding dimension parameter (see, e.g., the upper part of Fig. 8). I means increasing of less than 5% over the full range $10 \le E \le 20$. Data set 26 is the only one taken for a pressure of 6.5 Pa, detuning $\delta \approx 0$, and for a pump intensity 14 times above threshold. At this pressure three-level coherence effects are present and the dynamics of the laser is no longer Lorenz-like.

Data set No.	p	τ_c/T	D_2	$K_2 T \approx \lambda_+ T$	$\frac{K_2 T}{D_2 - 2} \approx \lvert\lambda_- T\rvert$	Remarks
7	19.4	525	1.03	0.018		P2;C
4	24.0	666	1.08	0.028		P2;C
8	20.0	531	1.23	0.046		P4;C
12	19.5	469	1.19	0.052		P4;C
23	23.1	1400	1.24	0.039		P8;C
24	21.4	24.3	1.79	0.33		P12;C
25	22.0	10.0	1.79	0.35		P2+P4;C
26	28.6	7.5	2.30	0.54	1.8	PDC;C
10	19.0	2.7	2.29	0.61	2.1	PDC;I
1	18.7	1.9	2.16	0.74	4.6	LC;WI
2	19.0	2.8	2.09	0.73	9.1	LC;C
3	24.8	2.6	2.15	0.63	5.5	LC;C
5	17.3	2.5	2.20	0.46	2.3	LC;WI
6	16.9	3.2	2.18	0.45	2.5	LC;I
13	16.7	5.6	2.18	0.37	2.1	LC;WI
14	15.2	4.9	2.06	0.18	2.7	LC;WI
15	17.5	5.8	2.04	0.40	10.6	LC;I
16	17.6	2.8	2.23	0.50	2.2	LC;WI
17	17.5	3.4	2.29	0.59	2.1	LC;I
18	21.8	3.2	2.11	0.37	3.4	LC;WI
19	17.3	3.5	2.07	0.44	6.2	LC;WI
20	17.0	2.7	2.12	0.51	4.2	LC;WI
21	21.9	4.4	2.15	0.27	1.8	LC;WI
22	20.3	3.5	2.02	0.47	20.3	LC;WI
	Numerical integration		2.033	0.70		Tuned, noise-free
	Numerical integration		2.055	0.69		Tuned+noise ($\sigma = 0.5$)
	Numerical integration		2.066	0.71		Detuned ($\delta = 0.05$)
	Caputo *et al.* (Ref. 25)			0.69		Numerical integration

able information.

Table I contains two columns connected with K_2 which has the inverse dimension of a time variable. That is why we calculated a dimensionless K_2 in terms of the average pulse period T as K_2T (see column 5). The sixth column uses a relation between K_2, the dimensions, and the Lyapunov exponents. If there is only one positive Lyapunov exponent, as is the case for the Lorenz model, $K_2 \approx \lambda_+$, where λ_+ is the positive Lyapunov exponent. If we accept the Kaplan-Yorke conjecture as valid, we obtain a relation between D and the Lyapunov exponents,

$$D = 2 + \lambda_+ / |\lambda_-| \ , \tag{4}$$

which yields an estimation for λ_-. Because D_2 is a lower bound of D and is near 2, this estimation of the Lyapunov exponents of our experimental data can give only a very rough approximation, but it is rather robust so long as the estimate of D is not too close to 2.0.

IV. LORENZ MODEL

The information, given in this paper, would not be complete if we did not compare our experimental results to theoretical data of the Lorenz-Haken model. For this purpose, we integrated numerically the equations of the Lorenz model[2,3] which are also appropriate for a single-mode laser with the homogeneously broadened two-level medium,

$$\begin{aligned} \frac{du}{dt} &= s(v-u) \ , \\ \frac{dv}{dt} &= ru - v - uw \ , \\ \frac{dw}{dt} &= uv - bw \ , \end{aligned} \tag{5}$$

to generate a set of data, comparable to at least one [see Fig. 2(a)] of our experimental data sets of Lorenz-type chaos. The variables (in laser physics) in (5) are the normalized inversion w, and the normalized amplitudes of the electric field u and of the atomic polarization v. Three parameters steer the behavior of the set (5) of equations: s is the cavity decay rate divided by the polarization decay rate ($x = \kappa/\gamma_\perp$), b is the population inversion decay rate divided by the polarization decay rate ($b = \gamma_\parallel/\gamma_\perp$), and r is the pumping rate, where $r = 1$ gives the lasing threshold. Integration was done by a double precision Runge-Kutta method with automatic adaptation of the integration step width.

An important point was to choose values for s, b, and r which would lead to a pulse train comparable to at least one of our experimental data sets of Lorenz-type chaos and which would be consistent with the experimental parameters. The pump rate r should be the same as in the experiments where we have estimated $r \approx 15$. The value for b was taken as $b = 0.25$.[19] It remained for us to estimate s. If we assume 4% round trip losses (an experimentally reasonable value), $\gamma_\perp \approx 1.6$ MHz (Ref. 29) for a pressure of 9 Pa, and 2 m as cavity length, we obtain $s \approx 2$. For this value of s we obtain a pulse train which appeared to be similar to our data set no. 3 (see trace a) of Fig. 2. 25 000 8-bit samples of the intensity u^2 were then taken from that pulse train.

Figures 7 and 8 show the result of the integration and of the data analysis. Part (a) of Fig. 7 contains the inversion w plotted versus the field u. It contains a trace of about 850 loops on the symmetric attractor. Typical Lorenz-like spirals of different length can be seen in part (b) where we plotted 5000 samples (≈ 175 pulses). The average number of samples per pulse is $p = 28.6$. Two phase portraits were made, one with delay 2 [part (c)] the other with delay 25 [part (d)]. They show again the hole of the attractor and the strange shape which projections of it can have. The center of the hole locates the unstable steady-state laser solution $u = \pm(r-1)^{1/2}$ and the hole itself indicates that the time-dependent solution in this case avoids that value. The autocorrelation function [part (e)] was calculated up to a delay of 4000 samples or about 140 average pulse lengths T. The slope of the correlation integral [part (f)] exhibits clear convergence with the embedding dimension E and a good plateau for the dimension estimation. The peaks again appear in the slope for higher $\ln(r)$ and are again somewhat enhanced by the use of the maximum norm but would have been also present with the use of the Euclidean norm.

The evaluation of the slopes and the differences of $\ln[C(r)]$ are presented in Fig. 8 from which we estimate $D_2 \approx 2.033$ and $K_2T \approx 0.70$. These values lie very well in the range of data found in Table I for Lorenz-type chaos. K_2T is also very similar to the value extracted from a theoretical investigation of Caputo and Atten[25] as can be seen in Table I.

As discussed in Sec. III experimental data clearly contain a certain unknown amount of noise. Its influence on experimental data could roughly be estimated by adding noise of different sizes to the theoretical data, performing the same dimension calculations as for the experimental data sets, and comparing to their results. Figure 9 shows the results for the "slope curves." We added Gaussian white noise with standard deviations σ of 0.0, 0.2, 0.5, and 1.0 in units of the least significant bit of the 8 bits used. The noise was added to the double precision data before rounding to 8-bit precision with the largest pulses nearly using the full 8 bits. One sees that the left part of the slope curve increases with increasing noise whereas the rest of the curve remains undisturbed. The comparison with experimental data (Fig. 4) reveals that the noise contained in those data is equivalent to $\sigma \approx 0.5$ which would be expected from the signal-to-noise ratio in our measurements. An analytical discussion of the influence of noise will be published elsewhere.[24]

For a further check of the robustness of the comparison between theoretical results to the measured data we included detuning by using the equations of Zeghlache and Mandel,[4]

$$\begin{aligned} \frac{du_1}{dt} &= -su_1 - sdu_2 + sv_1 \ , \\ \frac{du_2}{dt} &= -su_2 + sdu_1 + sv_2 \ , \end{aligned}$$

$$\frac{dv_1}{dt} = -u_1 w + r u_1 - v_1 + d v_2 \ , \tag{6}$$

$$\frac{dv_2}{dt} = -u_2 w + r u_2 - v_2 - d v_1 \ ,$$

$$\frac{dw}{dt} = u_1 v_1 + u_2 v_2 - b w \ ,$$

where w is the normalized inversion as before, u_1 and u_2 are real and imaginary prats of the normalized complex amplitude of the electric field, and v_1 and v_2 are real and imaginary parts of the normalized complex polarization. The detuning d is the normalized steady-state laser frequency detuning from the atomic resonance frequency $d=(\omega_A-\omega_L)/\gamma_\perp$, where ω_A mean the atomic and ω_L the laser frequency.

With the same values ($r=15$, $b=0.25$, and $s=2$) as before we found a wide period-3 "window" near $d\approx 0.155$, whereas for $d \lesssim 0.05$ we found Lorenz-type pulsing very similar to our data set no. 3 [see Fig. 2(a)] but with a bigger hole in the attractor. Even with this rather large detuning all other qualitative features differ only slightly from those of Fig. 7. Results for dimension and entropy are included in Table I for the noise-free data set in this detuned case. One is led to the conclusion that small detunings could have been present during our measurements of Lorenz-like spiral chaos that would not have led to noticeable differences from behavior in the

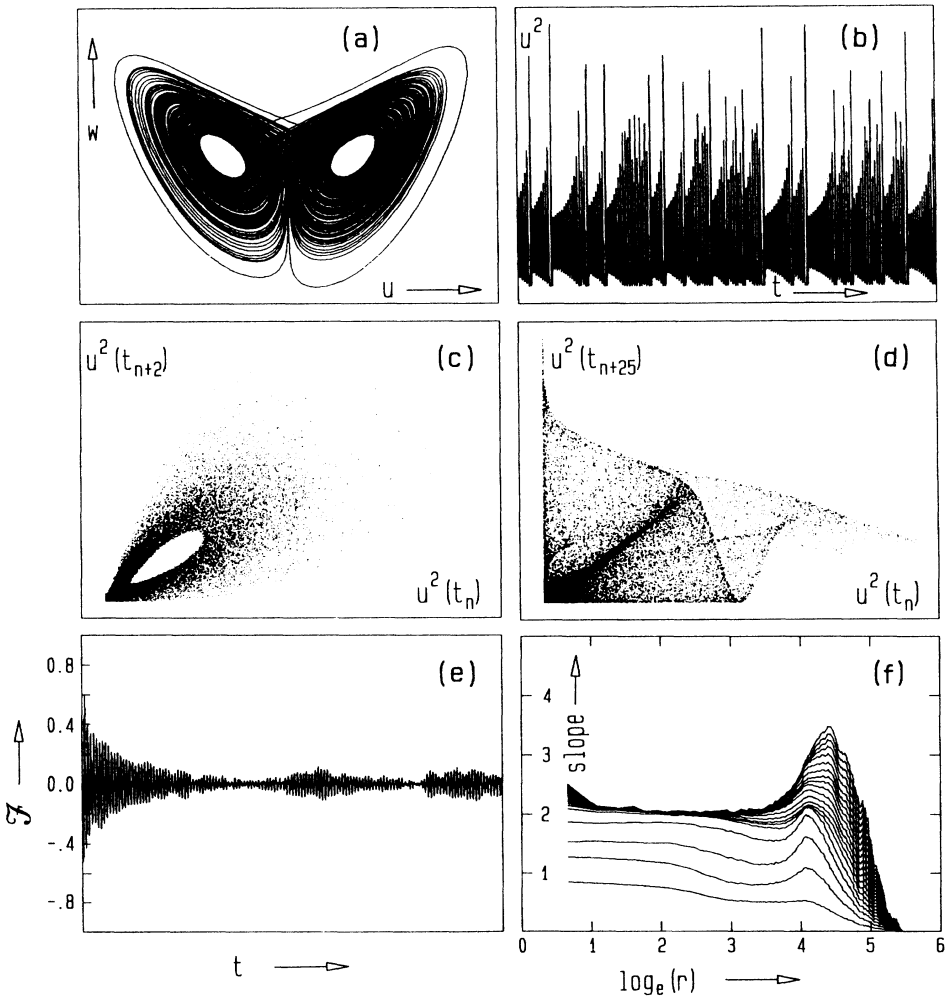

FIG. 7. Numerical results of the integrated Lorenz equations (Refs. 2 and 3) for parameters $r=15$, $b=0.25$, and $s=2$. (a) Inversion w vs the field u (about 850 loops). (b) Lorenz spirals of different lengths (5000 samples ≈ 175 pulses; average period $p\approx 28.6$). (c) Phase plot u_n vs $u_{n+k}, k=2$; (d) phase portrait for $k=25$. (e) Autocorrelation function (maximum delay $4000\approx 140T$). (f) Slopes of the log-log plots of the correlation integral for embedding dimensions 1 (lower curve) to 20 (upper curve) vs $\ln(r)$.

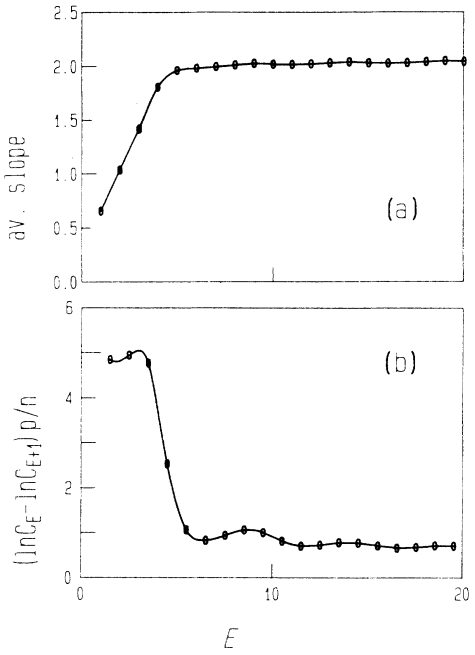

FIG. 8. (a) The correlation dimension D_2 and (b) K_2T taken as in Fig. 6 vs embedding dimension E for the data set of the numerically integrated Lorenz equations.

perfectly tuned case. This provides quantitative confirmation of the apparent similarity of the chaos in resonance and the chaos with small detuning which was noted by Zeghlache[30] and in Ref. 4.

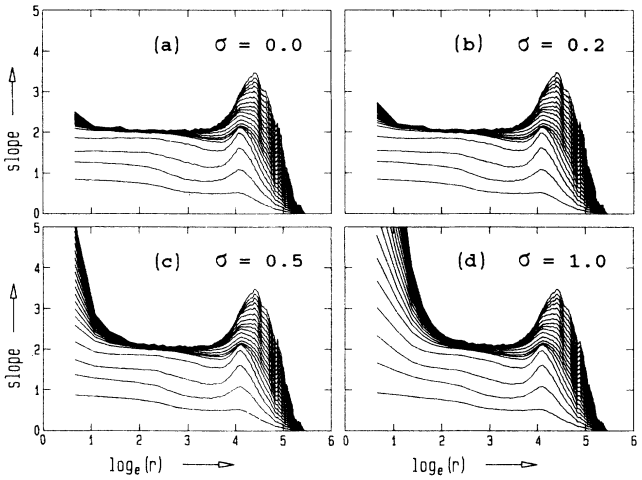

FIG. 9. Slope curves of the noisy numerically generated data sets calculated by integration of the Lorenz equations, then adding Gaussian noise of different standard deviations σ (values taken in units of the least significant bit) and then truncating the "noisy data" to 8 significant bits. In each of the four figure parts the lowest curve belongs to embedding dimension $E=1$ and the uppermost to $E=20$.

V. DISCUSSION

Lorenz-like spiral chaos exhibited in the intensity pulsing of FIR lasers has been shown to be relatively indistinguishable from the numerical simulations of chaotic solutions of the Lorenz model when comparisons are made between them in phase portraits, autocorrelation functions, and values of dimension (D_2) and entropy (K_2). One can thus conclude that these features of the experimental system are well described by the simple model. However, in the face of the numerous analyses of optically pumped (three-level) systems which claim to demonstrate that the Lorenz-Haken model is not sufficient to explain the behavior, one should be cautious in drawing absolute conclusions from the comparison so described. The measurement of these single quantities from the "spectra"[31] of D_q and K_q only indicates Lorenz-like behavior of the experimental three-level system and further studies of the full spectrum of these quanties are necessary for conclusive statements. Such studies are in progress.

As an alternative, phase-sensitive measurements[5] have recently been used to distinguish Lorenz-like chaotic pulsing from other types, based on the existence or absence of phase jumps by π radians between successive spirals. It is clear that the D_q's or K_q's calculated from intensity time series will not be sensitive to this difference because it occurs relative abruptly while the intensity is so close to zero that the subtleties may be impossible to resolve with finite accuracy. Hence, one is left to conclude that the quantitatively resolvable characteristics of these intensity time series are also Lorenz-like.

Some further comments about the values of D_2 and K_2 are in order.

We note that the D_2 values are consistently close to 2, which gives special features related to the nearly two-dimensional character of the attractor. One of these special features is that the attractor is efficiently reconstructed when $E_c n\Delta t \approx T$ if $E_c \geq 2D_2+1$. Hence, an efficient selection of $n\Delta t$ is $T/5$ (we have used $T/7$ with excellent efficiency of convergence). It is worth noting that we have not separately varied the "embedding time" (the spacing between components of any one vector given by $n\Delta t$) and the "attractor sampling time" (the spacing between first components of successive vectors). Independent variation of these two times may provide better rules of thumb for the application of the algorithms.

Furthermore, because $D_2 \approx 2$, the systematic errors introduced by the limited precision of the 8-bit data, can be sufficient to suppress D_2 below 2. This anomalous and sometimes controversial result (since $D_0 \geq 2$ for chaotic attractors it is often surprising when D_2 falls below 2 even though there is no lower bound for D_2) is avoided by applying the simple first-order correction procedure described in the text.

With $D_2 \approx 2$, there can be only one positive Lyapunov exponent which is given to a good accuracy by K_2. It is interesting to note that $K_2\tau_c \approx 1$, where τ_c is the decay time of the envelope of the autocorrelation function in the limit of short times. How universal this simple relation will be is unclear from other systematical analyses

reported to date.[32] However, it is clear that one may have to use a much larger embedding to find a convergent value for K_2. The evidence is that the required embedding dimension for this convergence is given by $En\Delta t \approx \tau_c \approx K_2^{-1}$ which for Lorenz-like spirals is of order $3-5T$. While similar values for K_2 and D_2 are found for period-doubling chaos and Lorenz-spiral chaos, other less "highly regarded" characterizations such as phase portraits and autocorrelation functions as well as, perhaps, return maps can more easily be used to distinguish them.

The discrepancy between the values of τ_c and K_2 in the periodic cases merit some discussion. Because of noise we find that τ_c is not infinite for these periodic cases and thus it is not surprising that K_2 is larger than zero. However, because τ_c is large we must also caution that our use of a maximum value of $E=20$ probably has not yet reached the conditions necessary for K_2 to fully converge.

Finally, we should remark on the use of an average of $C(r)$ over all points of the attractor before finding its scaling with r. For attractors with complex macroscopic structure (such as period-doubling cases) it may be necessary to take pointwise values of $C(r)$ (that is, centered on a particular point) in order to avoid spurious averaging of different length scales of the macroscopic structure in different portions of the attractor.

ACKNOWLEDGMENTS

This work was supported in part by Deutsche Forschungsgemeinschaft, a NATO collaborative research grant, and by a grant from the European Community. One of us (N.B.A.) was supported by the Alexander von Humboldt Foundation. We are pleased to acknowledge discussions and assistance with the data acquisition interfacing from W. Klische and valuable discussions on dimension and entropy calculations with F. Mitschke, M. Möller, W. Lange, G. Broggi, and A. M. Albano. We are also grateful for detailed discussions of characteristics of the Lorenz-Haken laser model with H. Zeghlache and P. Mandel.

*Permanent address: Department of Physics, Bryn Mawr College, Bryn Mawr, PA 19010.

[1](a) E. Hogenboom, W. Klische, C. O. Weiss, and A. Godone, Phys. Rev. Lett. **55**, 2571 (1985); (b) C. O. Weiss and J. M. Brock, *ibid.* **57**, 2804 (1986).

[2]E. N. Lorenz, J. Atmos. Sci. **20**, 130 (1963).

[3](a) A. V. Uspenskiy, Rad. Eng. Electron. Phys. **9**, 605 (1964); (b) V. V. Korobkhin and A. V. Uspenskiy, Zh. Eksp. Teor. Fiz. **45**, 1003 (1963) [Sov. Phys.-JETP **18**, 693 (1964)]; (c) A. Grasiuk and A. N. Oraevsky, in *Quantum Electronics and Coherent Light,* edited by P. Miles (Academic, New York, 1964), p. 192; (d) H. Haken, Phys. Lett. **53A**, 77 (1975).

[4](a) P. Mandel and H. Zeghlache, Opt. Commun. **47**, 146 (1983); (b) H. Zeghlache and P. Mandel, J. Opt. Soc. Am. B **2**, 18 (1985); (c) H. Zeglache, P. Mandel, N. B. Abraham, and C. O. Weiss, Phys. Rev. A **38**, 3128 (1988).

[5](a) C. O. Weiss, N. B. Abraham, and U. Hübner, Phys. Rev. Lett. **61**, 1587 (1988); (b) C. O. Weiss, W. Klische, N. B. Abraham, and U. Hübner, Appl. Phys. B **49**, 211 (1989).

[6]W. Klische and C. O. Weiss, Phys. Rev. A **31**, 4049 (1985).

[7]M. A. Dupertuis, R. R. E. Salomaa, and M. R. Siegrist, Opt. Commun. **57**, 410 (1986).

[8]J. C. Ryan and N. M. Lawandy, Opt. Commun. **64**, 59 (1987).

[9](a) J. S. Uppal, R. G. Harrison, and J. V. Moloney, Phys. Rev. A **36**, 4823 (1987); Phys. Rev. Lett. **59**, 2868 (1987); (b) W. Forysiak, R. G. Harrison, and J. V. Moloney, Phys. Rev. A **39**, 421 (1989); (c) J. V. Moloney, W. Forysiak, J. S. Uppal, and R. G. Harrison, *ibid.* **39**, 1277 (1989).

[10]P. A. Khandokhin, Ya. I. Khanin, and I. V. Koryukin, Opt. Commun. **65**, 367 (1988).

[11]F. Laguarta, T. Pujòl, R. Vilaseca, and R. Corbalan, J. Phys. (Paris) Colloq. Suppl. 6, **49**, C2-408 (1988).

[12](a) P. Grassberger and I. Procaccia, Phys. Rev. Lett. **50**, 346 (1983); (b) Phys. Rev. A **28**, 2591 (1983).

[13]A. Renyi, *Probability Theory* (North-Holland, Amsterdam, 1970).

[14](a) R. Badii and A. Politi, J. Stat. Phys. **40**, 725 (1985); (b) G. Broggi, J. Opt. Soc. Am. B **5**, 1020 (1988).

[15]*Dimensions and Entropies in Chaotic Systems,* edited by G. Meyer Kress (Springer, New York, 1986); R. Badii and A. Politi, in *Instabilities and Chaos in Quantum Optics II,* edited by N. B. Abraham, F. T. Arecchi, and L. A. Lugiato (Plenum, New York, 1988), p. 335.

[16]H. G. E. Hentschel and I. Procaccia, Physica D **8**, 435 (1983).

[17](a) M. Sano and Y. Sawada, Phys. Rev. Lett. **55**, 1082 (1985); (b) A. Wolf, J. Swift, H. L. Swinney, and J. Vastano, Physica D **16**, 285 (1985); (c) J. P. Eckmann, S. Ollifson Kamphorst, D. Ruelle, and S. Ciliberto, Phys. Rev. A **34**, 4971 (1986).

[18]R. Badii and A. Politi, Phys. Rev. A **35**, 1288 (1987).

[19]N. M. Lawandy and D. V. Plant, Opt. Commun. **59**, 55 (1986).

[20]Informations about the methods may be found, e.g., in (a) N. B. Abraham, A. M. Albano, B. Das, G. De Guzman, S. Yong, R. S. Gioggia, G. P. Puccioni, and J. R. Tredicce, Phys. Lett. A **114**, 217 (1986); (b) A. Brandstater and H. L. Swinney, Phys. Rev. A **35**, 2207 (1987); (c) L. A. Smith, Phys. Lett. A **113**, 283 (1988).

[21]N. B. Abraham, A. M. Albano, B. Das, and M. F. H. Tarroja, in *Fundamentals of Quantum Optics II,* edited by F. Ehlotsky (Springer, Berlin, 1987), p. 32.

[22]H. Froehling, J. P. Crutchfield, D. Farmer, N. H. Packard, and R. Shaw, Physica D **3**, 605 (1981).

[23]F. Takens, in *Non-Linear Dynamics and Turbulence,* edited by G. T. Barenblatt, G. Iooss, and D. Joseph (Pitman, London, 1985).

[24]M. Möller, F. Mitschke, W. Lange, N. B. Abraham, and U. Hübner, Phys. Lett. A **138**, 176 (1989).

[25]J. G. Caputo and P. Atten, Phys. Rev. A **35**, 1311 (1987).

[26]A. M. Albano, J. Muench, C. Schwartz, A. I. Mees, and P. E. Rapp, Phys. Rev. A **38**, 3017 (1988).

[27]*Instabilities and Chaos in Quantum Optics,* edited by F. T. Arecchi and R. G. Harrison (Springer, Berlin, 1987), p. 28.

[28](a) P. Grassberger, J. Stat. Phys. **26**, 173 (1981); (b) J. R. Tredicce, F. T. Arecchi, G. P. Puccioni, A. Poggi, and W. Gadomski, Phys. Rev. A **34**, 2073 (1986).

[29]J. R. R. Leite, M. Ducloy, A. Sanchez, D. Seligson, and M. S. Feld, Phys. Rev. Lett. **39**, 1469 (1977).

[30]H. Zeghlache, Ph.D. thesis (Bruxelles, 1988) (unpublished).
[31](a) H. G. E. Hentschel and I. Procaccia, Physica D **8**, 435 (1983); (b) T. C. Halsey, M. H. Jensen, L. P. Kadenoff, I. Procaccia, and B. Shraiman, Phys. Rev. A **33**, 1141 (1986); (c) K. Pawelzik and H. G. Schuster, *ibid.* **35**, 481 (1987).
[32](a) R. Badii, K. Heinzelmann, P. F. Meier, and A. Politi, Phys. Rev. A **37**, 1323 (1988); (b) I. McMackin, C. Radzewicz, M. Beck, and M. G. Raymer, *ibid.* **38**, 820 (1988).